Electronic Supplementary Material (ESI) for Inorganic Chemistry Frontiers.

Supporting Information

Catalytic Separator with Co–N–C Nanoreactor for High-Performance Lithium-Sulfur Batteries

*Longtao Ren,[a] Qian Wang,[b] Yajie Li,[a] Cejun Hu,[a] Yajun Zhao,[a] Lu Qiao,[a] Henghui Zhou,[b] Wen Liu, [*a] Haijun Xu[*a] and Xiaoming Sun [*a]*

[a] State Key Laboratory of Chemical Resource Engineering, Beijing Advanced Innovation Center for Soft Matter Science and Engineering, College of Chemistry, Beijing University of Chemical Technology, Beijing 100029, China
[b] College of Chemistry and Molecular Engineering, Peking University, Beijing 100871, China
[*]Corresponding author.
Email addresses: wenliu@mail.buct.edu.cn (W. Liu), hjxu@mail.buct.edu.cn (H. Xu), sunxm@mail.buct.edu.cn (X. Sun).

Contents

Supplementary Experimental

Materials characterization

The structure and morphology of the as-prepared samples were characterized using high-resolution transmission electron microscopy (HRTEM, JEOL JEM–2100, accelerating voltage=200 kV) and aberration-corrected high-angle annular darkfield scanning transmission electron microscope (HAADF-STEM, JEOL JEM–ARM200F, operated at 200 kV). The crystalline structures of all the samples were identified by using Shimadzu XRD–6000 diffractometer (Cu Kα source, λ = 1.5418 Å). X-ray photoelectron spectroscopy (XPS) was carried out on Thermo Electron ESCALAB 250. X-ray absorption fine structure (XAFS) measurement and data analysis: XAFS spectra at the Co K-edge were measured at the beamline 1W1B station of the Institute of high energy physics (Chinese academy of sciences, China). The Co K-edge XANES data of Co–N–C/AC was recorded in a fluorescence mode and the references (CoO and Co foil) were recorded in a transmission mode. The storage ring was operated at an energy of 2.5 GeV with an average electron current of 250 mA. The hard X-ray was monochromatized with Si (111) double-crystals. The obtained extended X-ray absorption fine structure (EXAFS) data were processed with the ATHENA module. The k^3-weighted EXAFS spectra in the k-space ranging from 2–10.5 $Å^{-1}$ were Fourier-transformed to real (R) space using hanging windows.

Symmetrical cell assembly and measurements

Symmetrical cells were fabricated with the standard 2032 coin-type by using two identical electrodes without sulfur loading, Celgard 2325 polypropylene membrane, and Co–N–C/AC modified membrane as the separator. CV measurements were performed between -0.8 V and 0.8 V at a scan rate of 5 mV s^{-1}. EIS spectra were recorded with scan frequency from 100 kHz to 0.01 Hz at open circuit potential on CHI 660 electrochemical workstation.

Computational Method

For each step of **Figure 5**, the reaction Gibbs free energy ΔG is defined by Eq. (1).

$$\Delta G = \Delta E + \Delta ZPE - T\Delta S \quad (1)$$

where ΔE is the binding energy, ΔZPE is the change in zero-point energy, T is the temperature, and ΔS is the entropy change. At low temperatures, the entropy contributions to ΔG are small, and the value of ΔS is set at zero. The binding energy between the Li_2S_x (x=8, 6, 4, 2, 1) and the substrate is defined by Eq. (2).

$$E_{binding} = E_{sub} + E_{Li2Sx} - E_{Li2Sx@sub} \quad (2)$$

where $E_{Li2Sx@sub}$ is the total energy of a substrate with an adsorbed Li_2S_x intermediate, E_{sub} is the total energy of substrates, and E_{Li2Sx} is the total energy of a single Li_2S_x intermediate in the vacuum. The initial state Li and S atom are deemed a bulk phase.

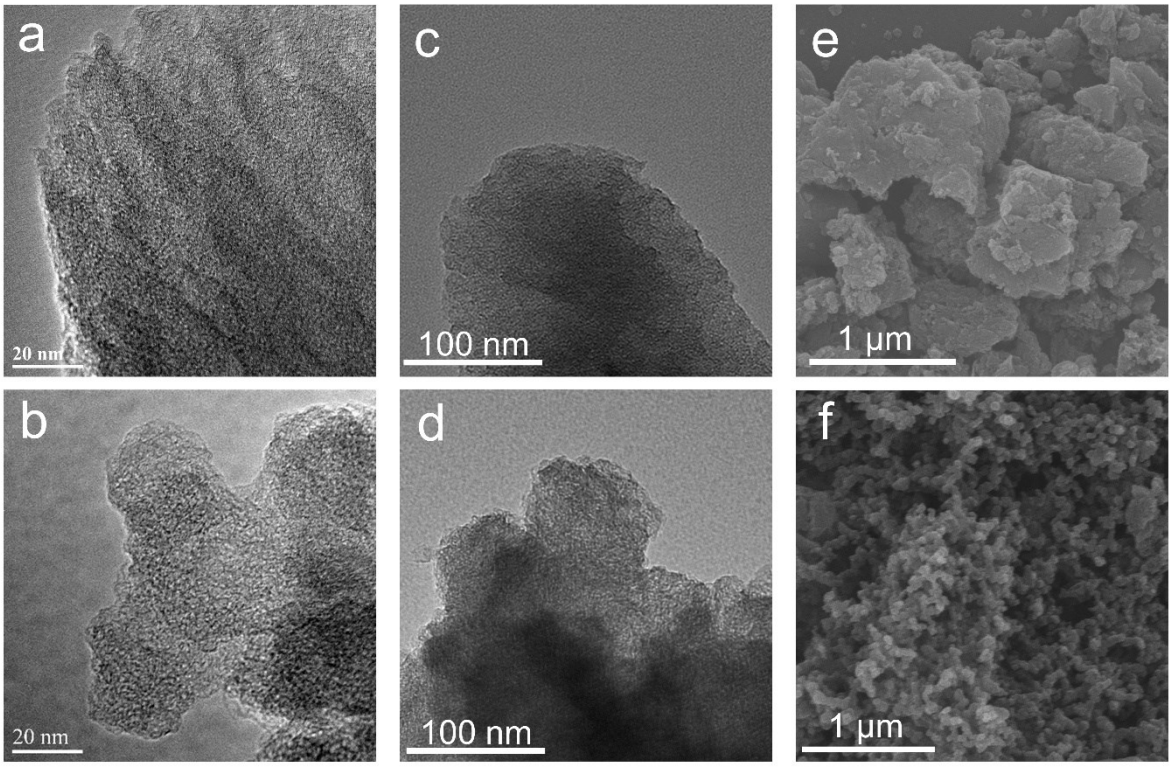

Figure S1. HRTEM images of (a) AC, (b) Co-N-C/AC. TEM images of (c) AC and (d) Co-N-C/AC. SEM images of (e) AC and (f) Co-N-C/AC.

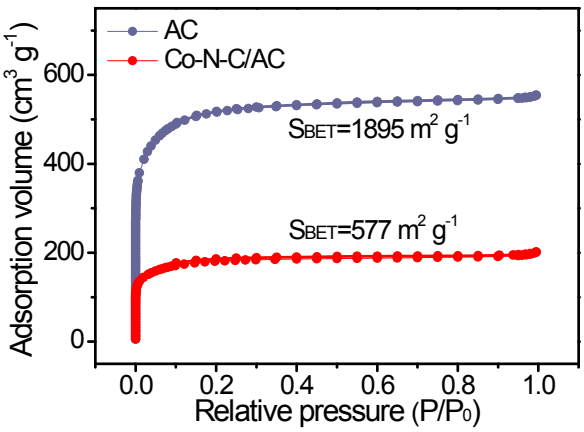

Figure S2. N2 adsorption-desorption analysis.

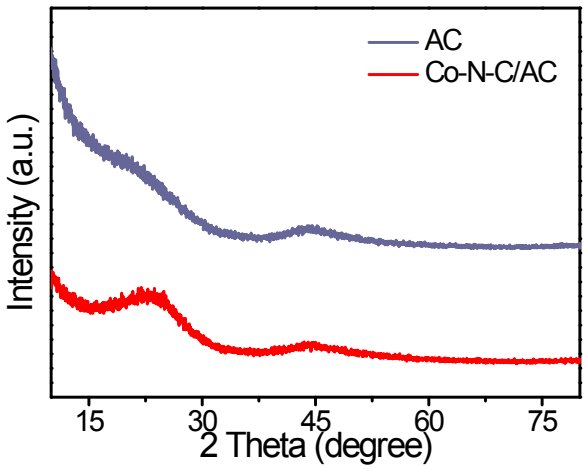

Figure S3. XRD pattern of AC and the Co–N–C/AC.

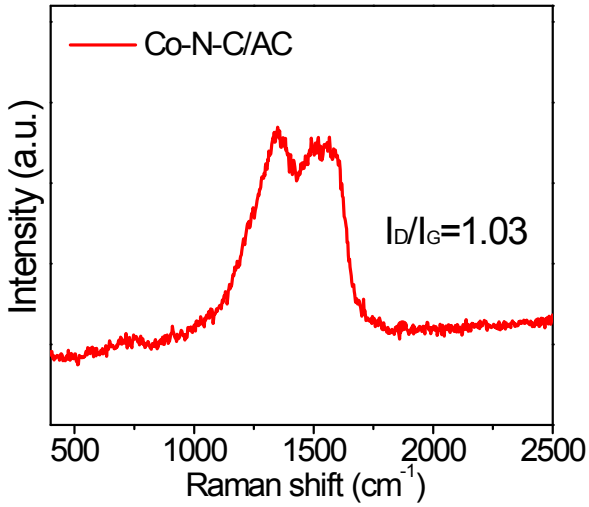

Figure S4. Raman spectra of Co-N-C/AC.

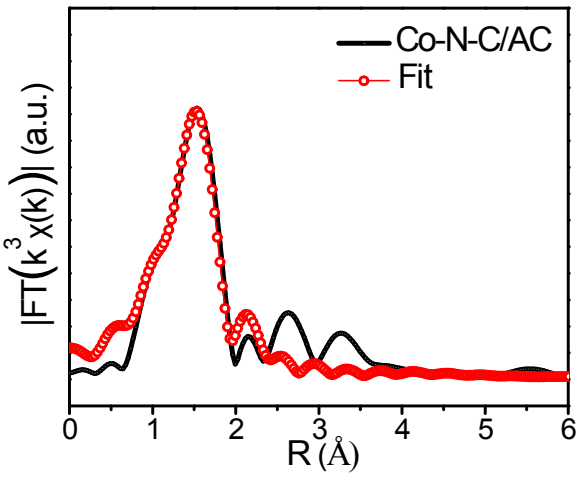

Figure S5. Corresponding EXAFS fitting curves of the Co–N–C/AC at *R* space.

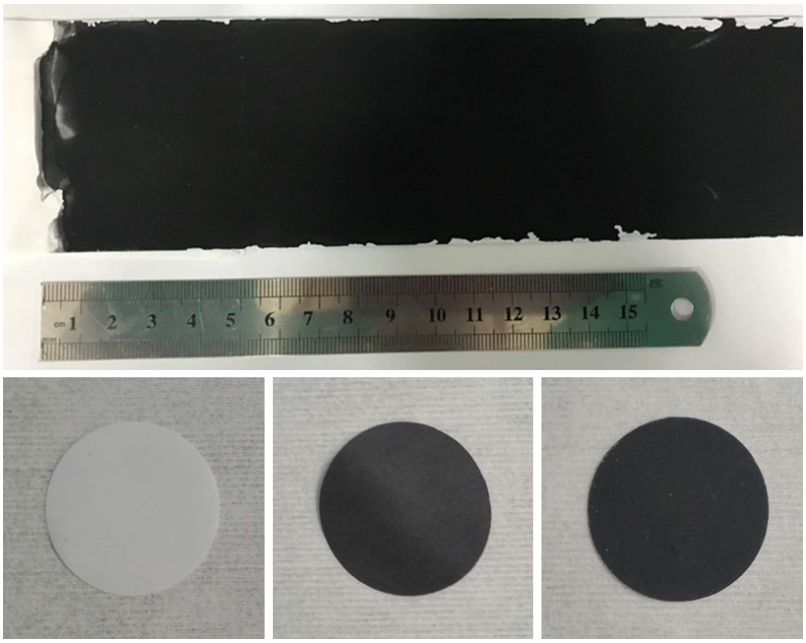

Figure S6. Photographs of the bare, N–C/AC, and Co–N–C/AC separators.

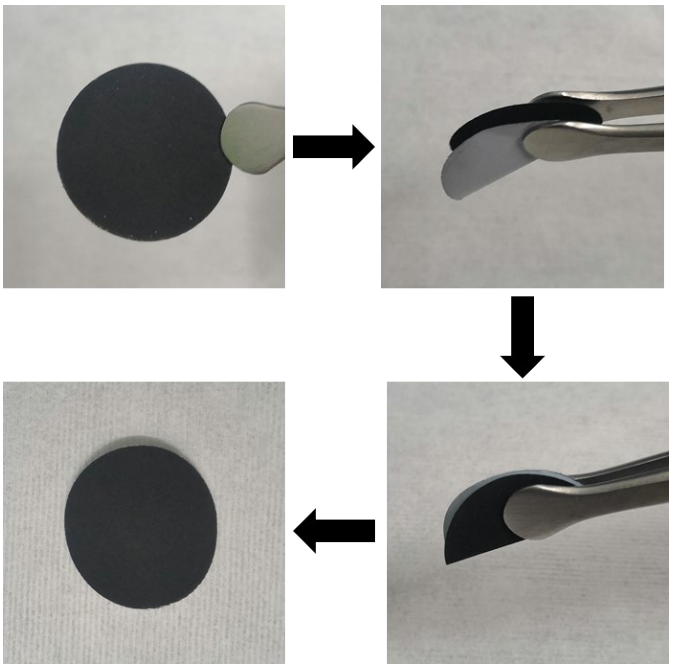

Figure S7. Co–N–C/AC modified separator at bending state and after recovery.

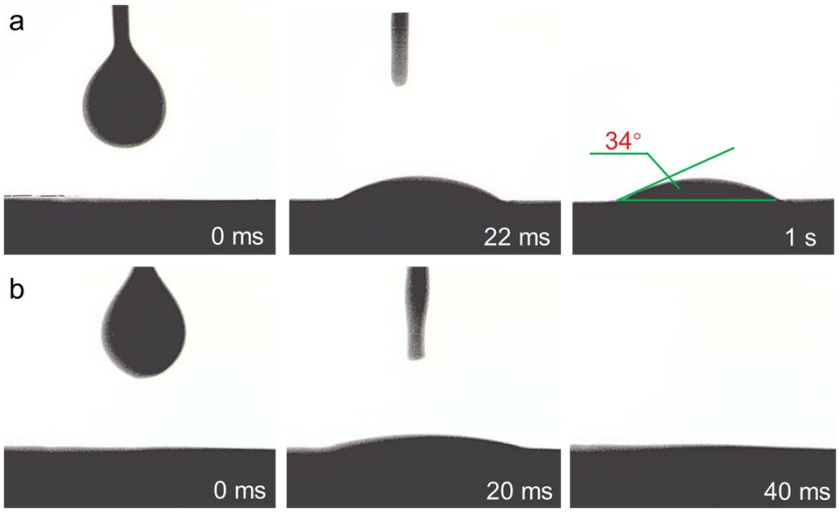

Figure S8. Contact angle measurement of Li–S electrolyte on the surface of (a) the bare and (b) Co-N-C/AC modified separators.

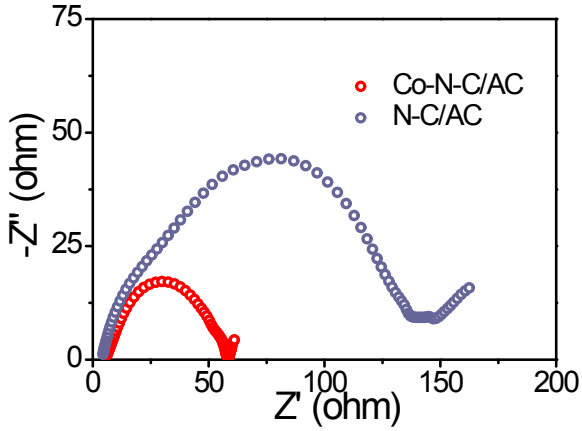

Figure S9. Electrochemical impedance spectra of the symmetric cells that based on the bare separator, the N–C/AC modified separator, and the Co–N–C/AC modified separator.

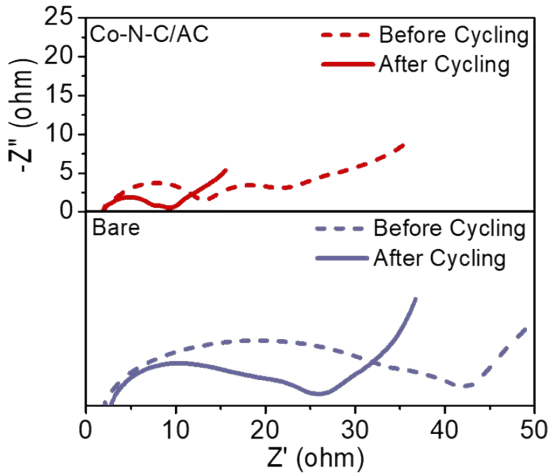

Figure S10. Electrochemical impedance spectra of the Li–S batteries based on the bare and the Co–N–C/AC modified separators before and after cycling.

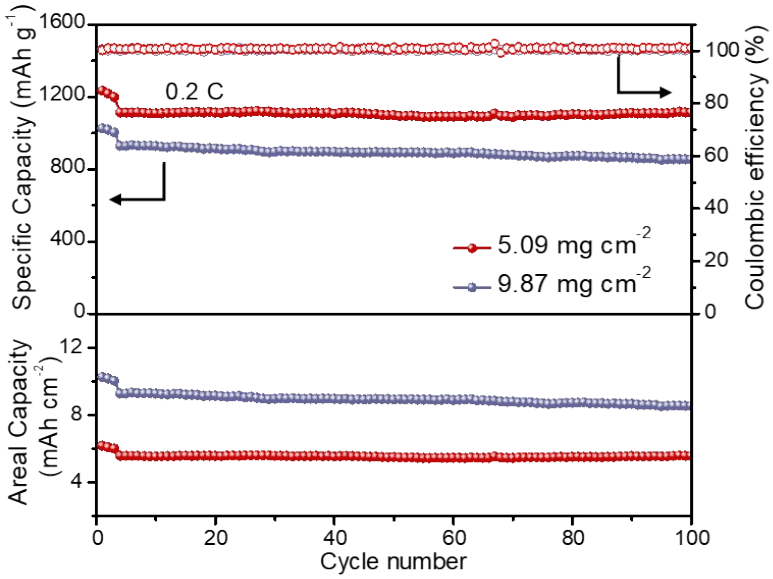

Figure S11. The cycling performance of the Li-S batteries based on the Co-N-C/AC modified separator with high-sulfur-loading in cathode.

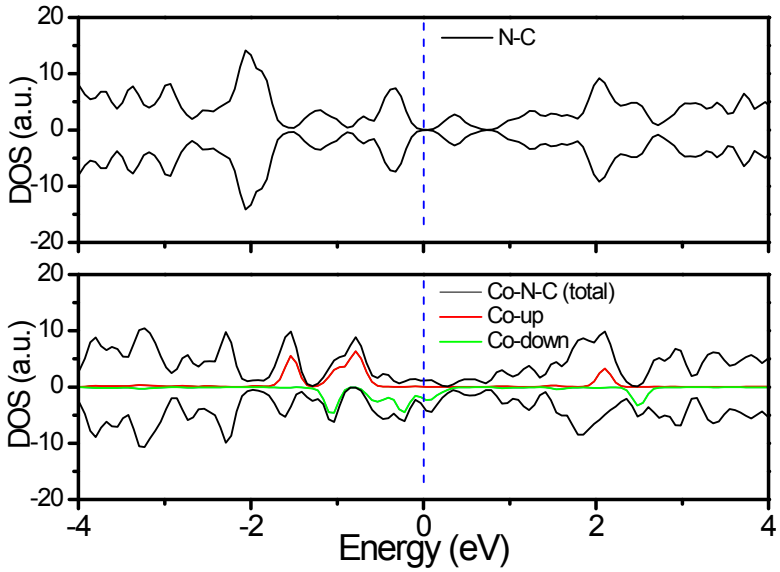

Figure S12. Density of states (DOS) diagrams of N–C, Co–N–C, and atomic projected DOS for Co atom. The Fermi levels (the vertical dashed line) are set to zero.

Table S1. EXAFS fitting parameters at the Co K-edge for Co-N-C/AC.

Sample	Path	C.N.	R(Å)	σ^2 ($\times 10^{-3}$Å^2)	R factor
Co-N-C/AC	Co-N	3.6	1.87	0.009	0.007

C.N. is the coordination number; R is the interatomic distance (the bond length between central atoms and surrounding coordination atoms); σ^2 is the Debye-Waller factor (a measure of thermal and static disorder in absorber-scatter distances). R factor is used to value the goodness of the fitting.

This value was fixed during EXAFS fitting, based on the known structure. Error bounds that characterize the structural parameters obtained by EXAFS spectroscopy were estimated as N ± 20%; R ± 1%; σ2 ± 20%; ΔE0 ± 20%. Co (FT range: 2.0-10.0 Å-1; fitting range: 0.8-2.8 Å)

Table S2. Electrochemical properties of various functional separators in Li-S batteries.

Materials	Mass loading of the coating (mg cm^{-2})	Sulfur Loading (mg cm^{-2})	Initial capacity (mAh g^{-1})	C Rated / Cycle Number	Capacity deacy (%)	Ref.
Ketjen Black	0.5	1.5-2.0	1350	0.5/500	0.09	1
Black Phosphorus	0.4	1.0-1.5	930	0.5/100	0.14	2
GO	0.12	1.5-2.0	920	0.1/500	0.23	3
MoS_2	-	-	808	0.5/600	0.083	4
Co_9S_8	0.16	-	869	1/1000	0.039	5
CNT@ZIF	0.9	1.2	1588.4	0.2/100	0.45	6
LDH/graphene	0.3	1.1-1.3	851	2/1000	0.06	7
CP/ $CoFe_2O_4$	-	1.72	733	1/1000	0.043	8
SC-Co	-	1.2	1130	0.5/300	0.086	9
Co-N_x@NPC/G	0.2	-	964	2/500	0.087	10
Co-N-C/AC	0.5	2.0	1169	1/500	0.043	This work

Table S3. Comparison of different rechargeable battery technologies with Li–S batteries.

Battery	Materials	Theoretical Specific Energy [W h kg^{-1}]	Capacity (mA h g^{-1})	Cycle Number	Capacity Retention (%)	Ref.
Li-ion	Li‖g-C_3N_4 /$LiCoO_2$	140	130	200	72.9	11
Na-S	Na‖Ni-MOF/S	760	598	1000	58	12
Zinc-ion	Zn‖D-MnO_2	820	388	500	-	13
Zn-O_2	Zn‖GNCNTs/O_2	1320	801	-	-	14
Li–O_2	Li‖GPE/PSSE/O_2	3500	1250	194	100	15
Li-S	Li‖Co-N-C/AC/S	2567	1169	500	78.8	This work

References

1 H. Yao, K. Yan, W. Li, G. Zheng, D. Kong, Z. W. Seh, V. K. Narasimhan, Z. Liang and Y. Cui, Improved lithium–sulfur batteries with a conductive coating on the separator to prevent the accumulation of inactive S-related species at the cathode–separator interface, *Energy Environ. Sci.,* 2014, **7**, 3381–3390.

2 J. Sun, Y. Sun, M. Pasta, G. Zhou, Y. Li, W. Liu, F. Xiong and Y. Cui, Entrapment of Polysulfides by a Black–Phosphorus-Modified Separator for Lithium–Sulfur Batteries, *Adv. Mater.,* 2016, **28**, 9797–9803.

3 J. Q. Huang, T. Z. Zhuang, Q. Zhang, H. J. Peng, C. M. Chen and F. We, Permselective Graphene Oxide Membrane for Highly Stable and Anti-Self-Discharge Lithium–Sulfur Batteries, *ACS Nano,* 2015, **9**, 3002–3011.

4 Z. A. Ghazi, X. He, A. M. Khattak, N. A. Khan, B. Liang, A. Iqbal, J. Wang, H. Sin, L. Li and Z. Tang, MoS2/Celgard Separator as Efficient Polysulfide Barrier for Long‐Life Lithium–Sulfur Batteries, *Adv. Mater.,* 2017, **29**, 1606817.

5 J. He, Y. Chen and A. Manthiram, Vertical Co9S8 hollow nanowall arrays grown on a Celgard separator as a multifunctional polysulfide barrier for high-performance Li–S batteries, *Energy Environ. Sci.*, 2018, **11**, 2560–2568.

6 F. Wu, S. Zhao, L. Chen, Y. Lu, Y. Su, Y. Jia, L. Bao, J. Wang, S. Chen and R. Chen, Metal-organic frameworks composites threaded on the CNT knitted separator for suppressing the shuttle effect of lithium sulfur batteries, *Energy Storage Mater.,* **2018**, *14*, 383–391.

7 H. J. Peng, Z. W. Zhang, J. Q. Huang, G. Zhang, J. Xie, W. T. Xu, J. L. Shi, X. Chen, X. B. Cheng and Q. Zhang, A Cooperative Interface for Highly Efficient Lithium–Sulfur Batteries, *Adv. Mater.,* 2016, **28**, 9551–9558.

8 X. H. Feng, Q. Wang, R. R. Li and H. Li, CoFe2O4 coated carbon fiber paper fabricated via a spray pyrolysis method for trapping lithium polysulfide in Li–S batteries, *Appl. Surf. Sci.,* 2019, **478**, 341–346.

9 Z. Cheng, H. Pan, J. Chen, X. Meng and R. Wang, Separator Modified by Cobalt–Embedded Carbon Nanosheets Enabling Chemisorption and Catalytic Effects of

Polysulfides for High–Energy–Density Lithium–Sulfur Batteries, *Adv. Energy Mater.,* 2019, **9**, 1901609.

10 J. Xie, B. Q. Li, H.J. Peng, Y. W. Song, M. Zhao, X. Chen, Q. Zhang and J. Q. Huang, Implanting Atomic Cobalt within Mesoporous Carbon toward Highly Stable Lithium–Sulfur Batteries, *Adv. Mater.,* 2019, **31**, 1903813.

11 Z. Lu, Q. Liang, B. Wang, Y. Tao, Y. Zhao, W. Lv, D. Liu, C. Zhang, Z. Weng, J. Liang, H. Li and Q. H. Yang, Graphitic Carbon Nitride Induced Micro-Electric Field for Dendrite-Free Lithium Metal Anodes, *Adv. Energy Mater.,* 2019, **9**, 1803186.

12 C. Ye, Y. Jiao, D. Chao, T. Ling, J. Shan, B. Zhang, Q. Gu, K. Davey, H. Wang and S. Z. Qiao, Electron−State Confinement of Polysulfides for Highly Stable Sodium−Sulfur Batteries, *Adv. Mater.,* 2020, **32**, 1907557.

13 J. Wang, J. G. Wang, X. Qin, Y. Wang, Z. You, H. Liu and M. Shao, Superfine MnO2 Nanowires with Rich Defects Toward Boosted Zinc Ion Storage Performance, *ACS Appl. Mater. Interfaces*, 2020, **12**, 34949−34958.

14 Y. Xu, P. Deng, G. Chen, J. Chen, Y. Yan, K. Qi, H. Liu and B. Y. Xia, 2D Nitrogen-Doped Carbon Nanotubes/Graphene Hybrid as Bifunctional Oxygen Electrocatalyst for Long-Life Rechargeable Zn–Air Batteries, *Adv. Funct. Mater,.* 2020, **30**, 1906081.

15 C. Zhao, Q. Sun, J. Luo, J. Liang, Y. Liu, L. Zhang, J. Wang, S. Deng, Xi. Lin, X. Yang, H. Huang, S. Zhao, L. Zhang, S. Lu and X. Sun, 3D Porous Garnet/Gel Polymer Hybrid Electrolyte for Safe Solid-State Li−O2 Batteries with Long Lifetimes, *Chem. Mater.*, 2020, **32**, 10113−10119.